Metrol. Meas. Syst., Vol. 31 (2024), No. 3
DOI: 10.24425/mms.2024.150292

METROLOGY AND MEASUREMENT SYSTEMS
Index 330930, ISSN 0860-8229
www.metrology.wat.edu.pl

IDENTIFICATION OF STEP-INDEX FIBERS BY STATIC LIGHT SCATTERING

Grzegorz Świrniak

Wroclaw University of Science and Technology, Department of Electronics, Photonics, and Microsystems, Chair of Electronic and Photonic Metrology, B. Prusa 53/55, 50-317 Wroclaw, Poland (✉ *grzegorz.swirniak@pwr.edu.pl*)

Abstract

The accurate characterization of optical fibers is crucial for numerous applications in telecommunications, sensing, and medical diagnostics. In this study, a novel method of sizing of step-index fibers is presented on the basis of the analysis of light scattering data. This approach integrates mathematical modeling of light scattering by step-index fibers with signal processing and correlation algorithms to extract information on the layered structure of the fiber under test. Practical measurements use of a novel optical system for laboratory-level tests. The results show a clear route to improve non-destructive and efficient fiber characterization in online industrial process control.

Keywords: optical fibers, scattering measurements, inverse scattering.

1. Introduction

In the realm of optical communication and sensing, step-index fibers play a pivotal role in facilitating efficient transmission of light signals [1-6]. The performance and reliability of step-index fibers are critically dependent on their structural and optical properties. For example, any variation in fiber diameter may lead to radiation loss and make fiber-to-fiber connections problematic. A technical verification of the characteristics of the fiber during the manufacturing process (in the fiber drawing stage) is of special importance [7, 8].

Characterization methods used for noncontact measurements of transparent fibers rely either on image projection or on scattering pattern analysis. In the first case, a beam of laser light is swept across the fiber at a constant time rate, and the fiber diameter is retrieved from a shadow registered by the detectors [7]. Nonimaging techniques, such as laser diffractometry [9-11], far-field resonance of forward scattered light [12, 13], spectral interferometry [14, 15], scattering near rainbow angle [16, 17], whispering gallery modes spectroscopy [18], and analysis of scattering effects by using standing wave illumination [19], involve estimations of the fiber characteristics from a mathematical analysis of the minima and maxima of scattering patterns. Alternatively, off-line microscopic or tomographic techniques can be used to study the characteristics of fibers in detail [7, 20, 21].

Here, a non-destructive technique is demonstrated that allows characterization of step-index fibers. Compared to commercial ‘shadowgraph instruments’ commonly used in the fiber industry for real-time outer diameter measurements and feedback control purposes [7], the technique offers the ability to retrieve diameters of the internal layers, provided that their refractive indices are known. This approach is based on *static light scattering* (SLS) of a polychromatic beam of light and a step-index FG050UGA optical fiber from Thorlabs, whose refractive index tomographic scan and profile are shown in Fig. 1. The fiber has a depressed clad design, *i.e.* the cladding consists of two regions: i) an inner cladding with the refractive

Copyright © 2024. The Author(s). This is an open-access article distributed under the terms of the Creative Commons Attribution-NonCommercial-NoDerivatives License (CC BY-NC-ND 4.0 http://creativecommons.org/licenses/by-nc-nd/4.0/), which permits use, distribution, and reproduction in any medium, provided that the article is properly cited, the use is non-commercial, and no modifications or adaptations are made.
Article history: received March 10, 2024; revised April 30, 2023; accepted May 16, 2024; available online August 2, 2024.

Early Access

index lower than the refractive index of the core, and ii) an outer cladding that has a higher refractive index than the inner cladding region.

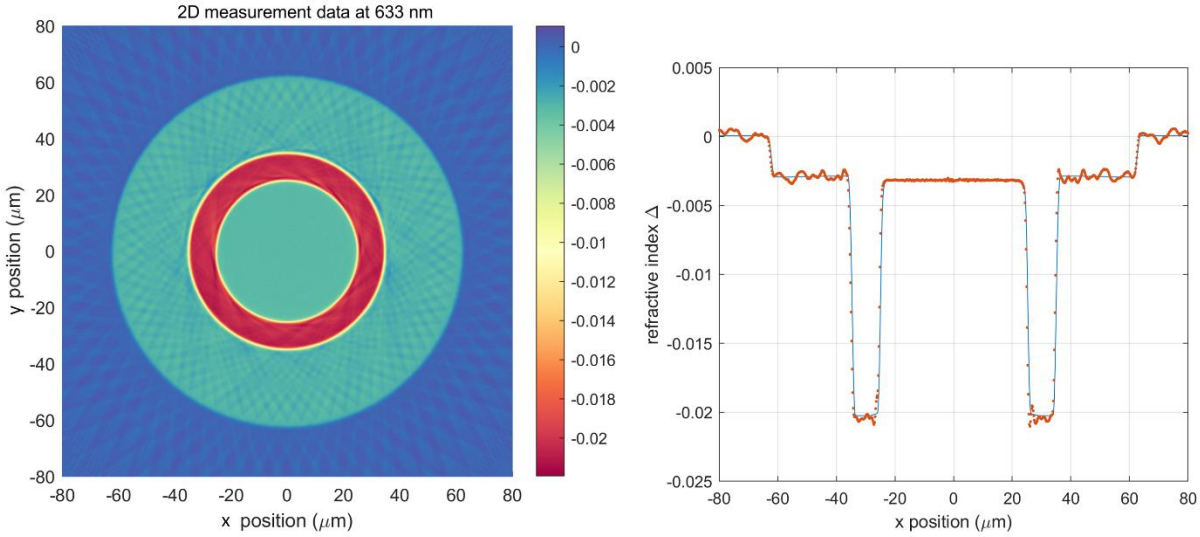

Fig. 1. Left: Tomographic image of a multimode, step-index Thorlabs FG050UGA fiber measured with an IFA-100 interferometric system; Right: the index profile inside the fiber (dots) and its average obtained by superposition of 360 tomographic projections taken at the step of 1° (solid). Refractive index units are Δn.

After this brief introduction, Section 2 summarizes the background of the SLS technique. Section 3 presents the data inversion method. An experimental setup for SLS measurements is introduced in Section 4, while measurement results are provided and discussed in Section 5. The paper ends with a conclusion section with perspectives for future improvements.

2. SLS background

SLS is particularly useful for determining the size of particles or macromolecules [22]. It is a noninvasive technique, meaning it does not require the alteration or labeling of the sample, which is advantageous for monitoring optical fibers online. SLS basically involves measurement of the intensity of light averaged over time at various spatial locations, which is shown schematically in Fig. 2. In this study, a polychromatic incident beam of light is used. This provides computational simplification when the measurement data is converted to the information on fiber properties and, importantly, reduces a detrimental sensitivity of measurement data to small changes in fiber properties [16, 23]. A polychromatic light beam can be viewed as a vector superposition of a number of mutually incoherent monochromatic fields propagating in the same direction and having a continuous distribution of angular frequencies $(\omega_{\min}, \omega_{\max})$:

$$\mathbf{E}^{\mathbf{inc}}(\mathbf{r},t) = \sum_{n=1}^{N} \mathbf{E}_n^{\mathbf{inc}}(t) \exp(\mathrm{i} k_n^{inc} \hat{\mathbf{n}}^{inc} \cdot \mathbf{r} - i\omega_n t), \tag{1}$$

where $\mathbf{r}$ is the position vector of the observation point (detector), $\mathbf{E}_n^{\mathbf{inc}}(t)$ is the complex amplitude of the electric field, which fluctuates randomly in time with the period long compared to the complex temporal term $\exp(-\mathrm{i}\,\omega_n t)$, and k_n^{inc} is the wave vector. The basic SLS equation transforms the incident monochromatic component $\mathbf{E}_n^{\mathbf{inc}}$ into the scattered one $\mathbf{E}_n^{\mathbf{sca}}$ upon its

Metrol. Meas. Syst., Vol. 31 (2024), No. 3
DOI: 10.24425/mms.2024.150292

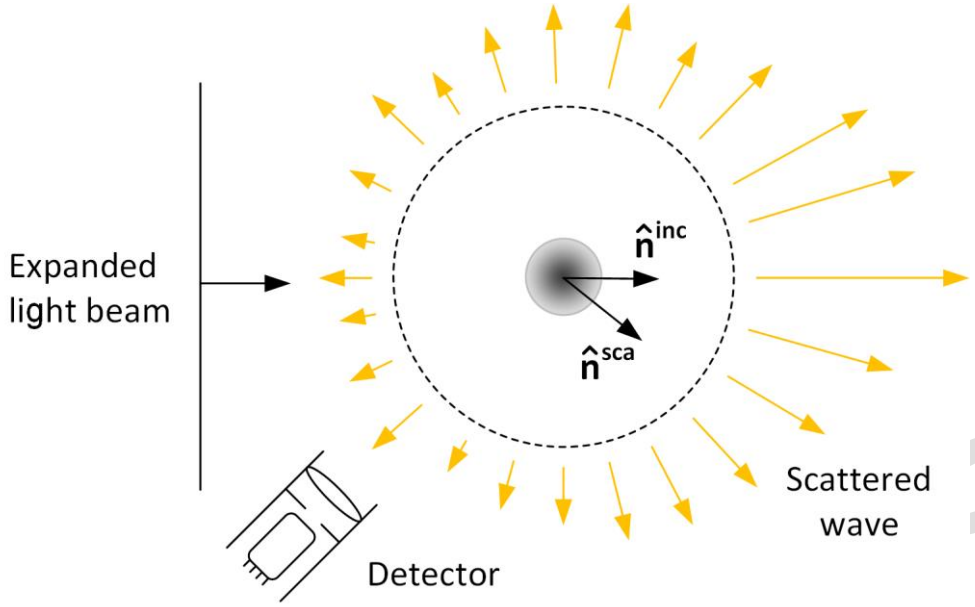

Fig. 2. Cross-section of a step-index optical fiber illuminated by a beam of well-formed light.

interaction with the fiber, using a separation-of-variables (SVM) solution of Maxwell's equations:

$$\begin{bmatrix} E_{\upsilon}^{sca}(\mathbf{r}) \\ E_{\varphi}^{sca}(\mathbf{r}) \end{bmatrix}_{r\to\infty} = \frac{e^{ik_0 r}}{r}\mathbf{S}(\hat{\mathbf{n}}^{\mathbf{sca}},\hat{\mathbf{n}}^{\mathbf{inc}}) \begin{bmatrix} E_{0\upsilon}^{inc} \\ E_{0\varphi}^{inc} \end{bmatrix}, \tag{2}$$

where $k_0 = 2\pi / \lambda_0$ is the wave number of the surrounding medium and $\mathbf{S}(\hat{\mathbf{n}}^{\mathbf{sca}},\hat{\mathbf{n}}^{\mathbf{inc}})$ is the 2×2 amplitude matrix which transforms the vector υ- and φ- components of the incident plane wave into the υ- and φ- components of the scattered wave. In general, the amplitude matrix depends on the fiber size, the refractive index profile, and the orientation with respect to the incident wave and the detector [24-26]. The time-averaged Poynting vector of the scattered electromagnetic field at a point $\mathbf{r}$ in space can be obtained by applying an additivity rule:

$$<< \mathbf{S}^{\mathbf{sca}}(\mathbf{r},t) >> = \mathrm{Re}\sum_{n=1}^{N} \mathbf{S}_n^{\mathbf{sca}}(\mathbf{r}), \tag{3}$$

where $<< ... >>$ denotes averaging over a long time interval and $\mathbf{S}_n^{\mathbf{sca}}$ is the complex Poynting vector of the n^{th} monochromatic component comprising the incident light:

$$\mathbf{S}_n^{\mathbf{sca}}(\mathbf{r}) = 1/2\,\mathbf{E}_n^{\mathbf{sca}}(\mathbf{r}) \times [\mathbf{H}_n^{\mathbf{sca}}(\mathbf{r})]^*, \tag{4}$$

with an asterisk denoting the complex conjugate. The scattered intensity in the far field, $I^{sca}(\mathbf{r})$, is the magnitude of the time-averaged Poynting vector. Finally, polychromatic illumination requires that the refractive index of each layer of the step-index optical fiber must be modeled as wavelength dependent:

$$m(\lambda) = (1 + \sum_{i=1}^{3} A_i \lambda^2 / (\lambda^2 - \ell_i^2))^{1/2} + \mathrm{i}\kappa + D, \tag{5}$$

where A_i, ℓ_i are the Sellmeier coefficients [27], κ is the attenuation constant at optical frequencies, and D is an offset to account for a dopant. For typical optical fibers, it is correct to assume that a dopant does not affect the shape of the fiber's dispersion curve $m(\lambda)$ [28].

Early Access

3. Data inversion

Data inversion relates the optical field back to properties of interest of the fiber. In this study, the diameters of the three refractive layers $d_1 < d_2 < d_3$, *i.e.* the core, the depressed cladding, and the cladding, are retrieved, as illustrated in the tomographic scan, Fig. 1. The inversion method involves correlations between two discrete space, real-valued signals, *i.e.*, a reference scattering signal $I_{ref}(\theta)$ and an experimental signal $I_{exp}(\theta)$. A database of reference signals is prepared only once by using the SLS theory introduced in Sect. 2 for various d_1, d_2 and d_3 corresponding to that which we expect to measure.

A quantitative comparison between the two signals I_{exp} and I_{ref} is made in a few steps. First, I_{ref} and I_{exp} are normalized since, in general, they differ in terms of the amplitude as well as the background offset:

$$\tilde{I}_{exp} = \frac{I_{exp} - \min\{I_{exp}\}}{\sum_{i=1}^{N}(I_{exp}(i) - \min\{I_{exp}\})}, \quad \tilde{I}_{ref} = \frac{I_{ref} - \min\{I_{ref}\}}{\sum_{i=1}^{N}(I_{ref}(i) - \min\{I_{ref}\})}, \tag{6}$$

where N refers to the number of data points. The background level was assumed to be independent of θ.

A quantitative comparison between $\tilde{I}_{exp}$ and $\tilde{I}_{ref}$ is realized by using a correlation estimator, defined as the weighted sum of squared errors of a prediction:

$$r^2(d_{1,2,3}) = \min_j \left\{ \frac{1}{N} \sum_{i=1}^{N} W(i)(\tilde{I}_{exp}(i+j) - \tilde{I}_{ref,\, d_{1,2,3}}(i))^2 \right\}, \quad \text{subject to} \quad j \in (\theta_1, \theta_2). \tag{7}$$

The term $\tilde{I}_{ref,\, d_{1,2,3}}$ denotes a normalized reference signal, which has been calculated for particular values of d_1, d_2 and d_3, while W is a vector of weighting coefficients that are equal to the variance of the experimental signal recorded without the presence of an optical fiber (*i.e.* the read noise of a detector). As $\tilde{I}_{exp}$ may undergo small angular shifts due to experimental uncertainties, the solution is found among a series of $\tilde{I}_{exp}$ shifted within the limits (θ_1, θ_2).

Finally, d_1, d_2 and d_3 are retrieved by minimizing the global residual (7):

$$\arg\min_{d_{1,2,3}} r^2(d_{1,2,3}), \qquad d_{1,2,3} \in H \subset \mathbb{R}^k, \tag{8}$$

where H is a *search region* on k = 3-dimensional domain determined by constraints and limits on the variables to be retrieved.

4. Experimental setup

An optical setup for SLS measurements of optical fibers is presented in Fig. 3. The fiber runs vertically through the middle of a 3-axis measurement stage. The integrated controller provides a fine rotation 0–180° about the fiber's main axis together with its vertical transitions along its length. A 14-bit CCD camera (Pixelfly, PCO AG) acquires weak optical signals and can be positioned at any angle θ = 0–180° ±0.01° with respect to the incident light. The illumination optics uses thermally stabilized red polychromatic light with the center wavelength of 630 nm and the spectral width (FWHM) of 14.5 nm. The polarization of the beam is adjusted parallel to the axis of the optical fiber. The beam is collimated, expanded, and filtered so that its cross section is about 7 mm^2. The fiber is side-illuminated at a normal angle.

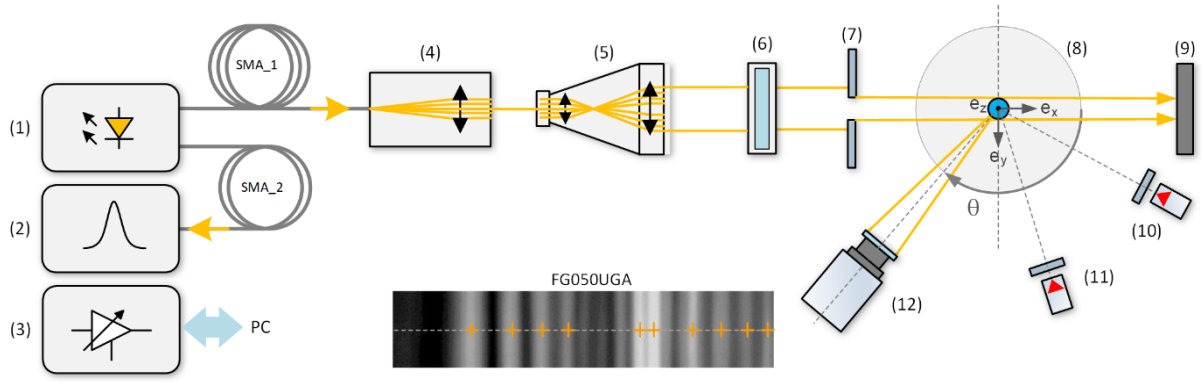

Fig. 3. Optical setup: (1) polychromatic illuminator, (2) spectrometer, (3) measurement platform controller, (4) fixed focus collimator, (5) beam expander, (6) linear polarizer, (7) spatial filter, (8) 3-axis measurement stage, (9) beam block, (10, 11) fiber alignment optics, (12) CCD 1392 × 1040 px camera.

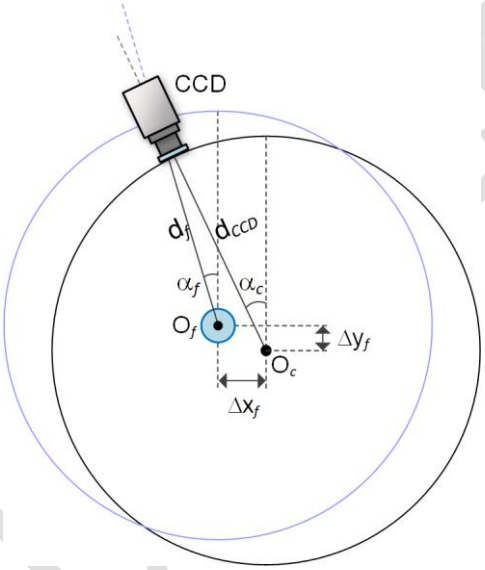

Fig. 4. An illustration of misalignment of the camera optical center (O_c) and the fiber axis (O_f).

In general, the fiber axis, O_f, does not coincide with the axis of rotation of a detector, O_d, as shown in Fig. 4. In particular, the CCD views at angle α_c rather than α_f which causes an image shift and affects the estimates. Fiber alignment optics uses two laser diodes and a CCD to determine the Δx_f and Δy_f misalignments by analyzing pairs of CCD images recorded at different camera viewing angles.

A Matlab-based software combines multiple images taken at successive angular positions. Each measurement is followed by a calibration procedure which removes unwanted data bias caused by the fiber misalignment effects. Then the CCD capture is subjected to a simple denoising procedure by using an average over rows of the CCD image.

5. Results and discussion

For the purposes of inverse studies, a database of reference signals was prepared for various operating conditions: d_3 = 120, 120.5,…, 130 μm, d_2 = 65, 65.5,…, 75 μm, d_1 = 45, 45.5 ,…, 55 μm. The database contains 21^3 = 9261 reference signals. Figure 5 compares the SLS

measured signal (solid) with the reference signal (dotted line) estimated by the inversion algorithm. The plot shows scattering in the vicinity of so-called 'primary rainbows', caused by light that has been subjected to one internal reflection [29]. The fiber under test was roughly characterized by the vendor with an outer cladding diameter of 125 +1/-2 μm, the core diameter 50 ± 1 μm. The core was made of pure silica glass, characterized by a refractive index of n = 1.457 at 633 nm [30], while the cladding was fluorine doped to decrease the refractive index. The closest agreement between the measurement and the reference signals was achieved for d_3 = 124.0 μm, $d_2 = 70.0$ μm, and $d_1 = 50.0$ μm. Notably, there are slight deviations between amplitudes of compared signals as the assumed and real experimental conditions differ; however, the angular positions of the extremes are in close agreement, which confirms the SLS modeling assumptions from Sect. 2.

Figure 6 shows how the r^2 function evaluates as the d_3 and d_1 vary while d_2 is kept constant (left panel) and d_3, d_2 vary, d_1 – constant (right panel). Note that both diagrams show well-defined local minima that correspond to estimated diameter values. Here the 'stability' of the r^2 plots is due to the fact, that for polychromatic light beams, the scattered signal does not reveal high-frequency ripples or resonance effects, typical for coherent illumination [29]. The r^2 function is also pretty sensitive to measured diameters. This manifests the ability of the method to retrieve the diameters of interest with much better accuracy.

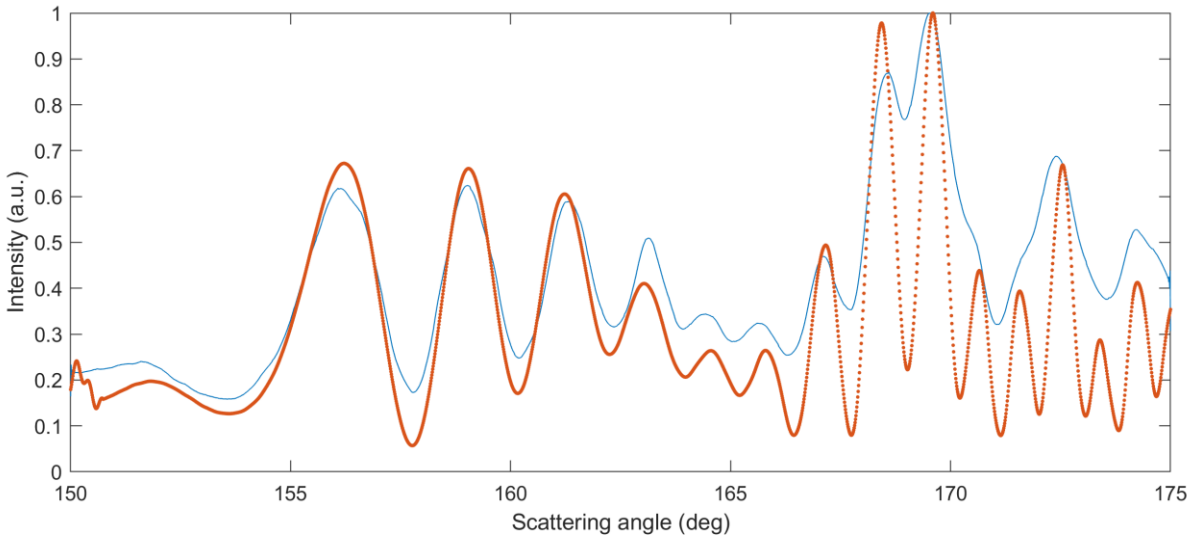

Fig. 5. SLS measured signal (solid) versus reference signal (dots) as estimated by the inversion algorithm; both normalized. The best match achieved for: $d_3 =$ 124.0 μm, $d_2 =$ 70.0 μm, $d_1 =$ 50.0 μm. Experimental data at: 633 nm, FWHM = 14.5 nm.

Metrol. Meas. Syst., Vol. 31 (2024), No. 3
DOI: 10.24425/mms.2024.150292

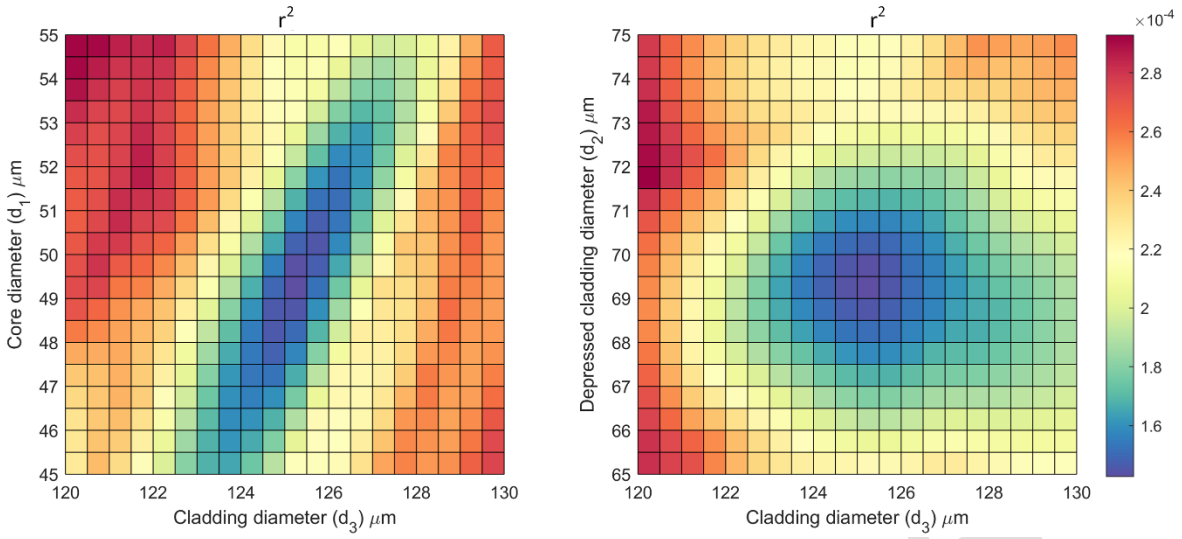

Fig. 6. Diagrams of the r^2 function where (left) the diameter d_2 of the depressed layer is fixed to 70.0 μm (left), and the core diameter d_1 is fixed to 50.0 μm (right).

6. Conclusions and perspectives

Practical tests demonstrated that the SLS technique supported by the data inversion algorithm based on the correlation between signals can be successfully applied to noninvasive measurements of step-index optical fibers. The method is able to retrieve internal diameters of fiber layers (core, inner- and outer cladding) and can be easily adopted to characterize step-index fibers of other complicated structures (*e.g.*, straight core/cladding, trench-assisted, with nanostructure ring, *etc.*) or capillary tubes with or without fluid [31].

Practical measurements using polychromatic light are rather nonstandard as the vast majority of SLS-based techniques use laser beams. This improves the stability of the inverse problem (which relates measurements back to the fiber properties of interest), since the SLS measurement data is detrimentally sensitive to small changes in fiber properties with monochromatic illumination [16, 23]. Nevertheless, the detection of weak rainbow signals for polychromatic light sources is a challenge.

The method is rather abstractive in terms of precise quantitative understanding of what is happening in the scattered field; therefore, one cannot derive accurate formulas for converting measurements to fiber properties of interest. Deep studies of scattering in layered fibers show that a simple physical interpretation of scattering for such complicated cases is decidedly non-trivial [29].

The next steps will be focused on assessing measurement errors of the method by means of statistical considerations. The primary concern here will be deviations of the fiber shape from perfectly axial. A promising perspective for the present study is that some machine learning algorithms that are capable of reducing the numerical effort by using various parallelization schemes can be easily adopted for efficient signal correlation.

References

[1] Flusberg, B. A., Cocker, E. D., Piyawattanametha, W., Jung, J. C., Cheung, E. L. M., & Schnitzer, M. J. (2005). Fiber-optic fluorescence imaging. *Nature Methods*, *2*(12), 941–950. https://doi.org/10.1038/nmeth820

[2] Kisała, P., Kalizhanova, A., Kozbakova, A., & Yeraliyeva, B. (2023). Identification of cladding modes in SMF-28 fibers with TFBG structures. *Metrology and Measurement Systems*, *30*(3), 507–518. https://doi.org/10.24425/mms.2023.146418

[3] Harasim, D., & Cięszczyk, S. (2022). A novel method of elimination of light polarization cross sensitivity on tilted fiber Bragg grating bending sensor. *Metrology and Measurement Systems*, *29*(4), 737–749. https://doi.org/10.24425/mms.2022.143066

[4] Boffi, P., Martelli, P., Gatto, A., & Martinelli, M. (2013). Mode-division multiplexing in fibre-optic communications based on orbital angular momentum. *Journal of Optics*, *15*(7), 075403. https://doi.org/10.1088/2040-8978/15/7/075403

[5] Tatarczak, A., Usuga, M. A., & Tafur Monroy, I. (2015). OAM-enhanced transmission for multimode short-range links. In A. K. Srivastava (Ed.), *Next-Generation Optical Networks for Data Centers and Short-Reach Links II*. SPIE. https://doi.org/10.1117/12.2079795

[6] Kisała, P. (2022). Physical foundations determining spectral characteristics measured in Bragg gratings subjected to bending. *Metrology and Measurement Systems*, *29*(3), 573–584. https://doi.org/10.24425/mms.2022.142275

[7] Marshall, G. F. (2012). *Handbook of Optical and Laser Scanning*, Marcel Dekker, New York. https://doi.org/10.1201/9781315218243

[8] Markos, C. (2014). Mapping the structure. *Nature Photonics*, *9*(1), 9–11. https://doi.org/10.1038/nphoton.2014.308

[9] Onofri, F., Lenoble, A., Bultynck, H., & Guéring, P.-H. (2004). High-resolution laser diffractometry for the on-line sizing of small transparent fibres. *Optics Communications*, *234*(1–6), 183–191. https://doi.org/10.1016/j.optcom.2004.02.026

[10] Lebrun, D. (1996). Enhancement of wire diameter measurements: comparison between Fraunhofer diffraction and Lorenz-Mie theory. *Optical Engineering*, *35*(4), 946. https://doi.org/10.1117/1.600703

[11] Khodier, S. A. (2004). Measurement of wire diameter by optical diffraction. *Optics & Laser Technology*, *36*(1), 63–67. https://doi.org/10.1016/s0030-3992(03)00134-8

[12] Watkins, L. S. (1974). Scattering from side-illuminated clad glass fibers for determination of fiber parameters. *Journal of the Optical Society of America*, *64*(6), 767. https://doi.org/10.1364/josa.64.000767

[13] Jianbing Wu. (n.d.). Study on the diameter measurement of optical fibers using the method of forward near-axis far-field interference. *IMTC/98 Conference Proceedings. IEEE Instrumentation and Measurement Technology Conference. Where Instrumentation Is Going (Cat. No.98CH36222)*. https://doi.org/10.1109/imtc.1998.676904

[14] Jasapara, J. C. (2005). Non-invasive characterization of microstructured optical fibers using Fourier domain optical coherence tomography. *Optics Express*, *13*(4), 1228. https://doi.org/10.1364/opex.13.001228

[15] Jasapara, J., Monberg, E., DiMarcello, F., & Nicholson, J. W. (2003). Accurate noncontact optical fiber diameter measurement with spectral interferometry. *Optics Letters*, *28*(8), 601. https://doi.org/10.1364/ol.28.000601

[16] Świrniak, G. (2020). Non-invasive mesurements of transparent fibres. *Metrology and Measurement Systems*, *27*(1), 19–31. https://doi.org/10.24425/mms.2020.131714

[17] Han, X., Ren, K. F., Wu, Z., Corbin, F., Gouesbet, G., & Gréhan, G. (1998). Characterization of initial disturbances in a liquid jet by rainbow sizing. *Applied Optics*, *37*(36), 8498. https://doi.org/10.1364/ao.37.008498

[18] Kavungal, V., Farrell, G., Wu, Q., Kumar Mallik, A., & Semenova, Y. (2018). Studies of geometrical profiling in fabricated tapered optical fibers using whispering gallery modes spectroscopy. *Optical Fiber Technology*, *41*, 82–88. https://doi.org/10.1016/j.yofte.2018.01.007

[19] Michihata, M., Zheng, Z., Funaiwa, D., Murakami, S., Kadoya, S., & Takahashi, S. (2021). In-Process Diameter Measurement Technique for Micro-Optical Fiber with Standing Wave Illumination. *Nanomanufacturing and Metrology*, *4*(1), 28–36. https://doi.org/10.1007/s41871-020-00081-4

[20] Fernandes, L. A., Sezerman, O., Best, G., Ng, M. L., & Kane, S. (2016). Direct writing of fiber optic components in photonic crystal fibers and other specialty fibers. In A. Heisterkamp, P. R. Herman, M. Meunier, & S. Nolte (Eds.), *SPIE Proceedings*. SPIE. https://doi.org/10.1117/12.2213597

[21] Yablon, A. D. (2009). Multi-Wavelength Optical Fiber Refractive Index Profiling by Spatially Resolved Fourier Transform Spectroscopy. *Optical Fiber Communication Conference and National Fiber Optic Engineers Conference*. https://doi.org/10.1364/ofc.2009.pdpa2

[22] Xu, R. (2002). Particle Characterization: Light Scattering Methods. In B. Scarlett (Ed.), *Particle Technology Series*. Springer Netherlands. https://doi.org/10.1007/0-306-47124-8

[23] Świrniak, G., & Mroczka, J. (2016). Approximate solution for optical measurements of the diameter and refractive index of a small and transparent fiber. *Journal of the Optical Society of America A*, *33*(4), 667. https://doi.org/10.1364/josaa.33.000667

[24] Gurwich, I., Shiloah, N., & Kleiman, M. (1999). The recursive algorithm for electromagnetic scattering by tilted infinite circular multilayered cylinder. *Journal of Quantitative Spectroscopy and Radiative Transfer*, *63*(2–6), 217–229. https://doi.org/10.1016/s0022-4073(99)00017-5

[25] Li, R., Han, X., Jiang, H., & Ren, K. F. (2006). Debye series of normally incident plane-wave scattering by an infinite multilayered cylinder. *Applied Optics*, *45*(24), 6255. https://doi.org/10.1364/ao.45.006255

[26] Renxian, L., Xiang'e, H., & Fang, R. K. (2009). Debye series expansion of shaped beam scattering by GI-POF. *Optics Communications*, *282*(22), 4315–4321. https://doi.org/10.1016/j.optcom.2009.07.054

[27] Fleming, J. W. (1984). Dispersion in GeO2–SiO2 glasses. *Applied Optics*, *23*(24), 4486. https://doi.org/10.1364/ao.23.004486

[28] Butov, O. V., Golant, K. M., Tomashuk, A. L., van Stralen, M. J. N., & Breuls, A. H. E. (2002). Refractive index dispersion of doped silica for fiber optics. *Optics Communications*, *213*(4–6), 301–308. https://doi.org/10.1016/s0030-4018(02)02087-4

[29] Świrniak, G., & Mroczka, J. (2017). Numerical analysis of primary rainbows from a homogeneous cylinder and an optical fiber for incident low-coherent light. *Journal of Quantitative Spectroscopy and Radiative Transfer*, *195*, 176–188. https://doi.org/10.1016/j.jqsrt.2017.01.009

[30] Malitson, I. H. (1965). Interspecimen Comparison of the Refractive Index of Fused Silica. *Journal of the Optical Society of America*, *55*(10), 1205. https://doi.org/10.1364/josa.55.001205

[31] Fitt, A. D., Furusawa, K., Monro, T. M., Please, C. P., & Richardson, D. J. (2002). *Journal of Engineering Mathematics*, *43*(2/4), 201–227. https://doi.org/10.1023/a:1020328606157

Grzegorz Świrniak is a graduate of the Faculty of Electronics at the Wrocław University of Science and Technology. He is now an Associate Professor at the Department of Electronics, Photonics and Microsystems. In his scientific work, he deals with optoelectronic metrology of synthetic and biological structures. He also studies the inverse problem in the scattering, absorption and emission of radiation by small particles.

Early Access